

# Gait analysis of athletes based on fiber optic sensors and computer vision algorithms

Nina Liu (✉ [liunina100978@163.com](mailto:liunina100978@163.com))  
Chongqing Creation Vocational College


---

## Research Article

**Keywords:** fiber optic sensor, Computers, Visual algorithms, Gait analysis

**Posted Date:** January 15th, 2024

**DOI:** <https://doi.org/10.21203/rs.3.rs-3852387/v1>

**License:**  This work is licensed under a Creative Commons Attribution 4.0 International License.  
[Read Full License](#)

**Additional Declarations:** No competing interests reported.

---

# Abstract

Walking may seem simple, but it actually involves complex control processes. Walking is accomplished through a series of collaborative operations, including coordinated control, balance control, central command, and various other physiological mechanisms. When problems arise between these links, it may cause abnormal gait or motor injury. Gait analysis of athletes can help coaches and medical personnel evaluate their athletic skills and physical health. Therefore, this article aims to develop an effective athlete gait analysis method based on fiber optic sensors and computer vision algorithms. Fiber optic sensors capture subtle changes in athletes' gait by measuring the changes in optical signals in the fiber optic. The collected gait data includes parameters such as stride length, stride frequency, and gait phase. Step length refers to the distance traveled during a walk, providing detailed information about an athlete's gait and helping to evaluate their athletic skills and physical health. Using computer vision algorithms to process and analyze the collected gait data, accurate gait parameters are obtained for identifying athletes' walking patterns and identifying abnormal gait.

## 1 Introduction

Gait analysis is a branch of the discipline that studies the laws of human walking motion (Silva and Stergiou 2020). The beginning of this field can be traced back to the 1990s. It provides objective and quantitative evaluation of walking function by utilizing a series of parameters such as time, geometry, mechanics, and electromyography to observe and analyze the kinematics of limb and joint activities during human walking. Gait analysis can be applied in many fields, such as sports training, rehabilitation medicine, medical diagnosis, and structural engineering (Baker et al. 2016). By analyzing motion related diseases and their association with gait, prediction and later treatment assistance can be made. Gait recognition technology based on computer vision can make gait analysis faster, more accurate, and more objective (Manssor et al. 2021). By modeling and analyzing video image data during exercise, the gait recognition system can extract features such as athlete's posture, contour, speed, and period, achieving precise recognition of gait (Verlekar et al. 2017). This technology has a wide range of applications in gait recognition, including gait recognition, disease prediction, rehabilitation plan formulation, etc., and has become an important technical means in the field of gait analysis.

The combination of fiber optic sensors and computer vision algorithms can achieve comprehensive analysis and evaluation of athlete gait, providing scientific basis and guidance for athlete rehabilitation, health care, and training. Fiber optic sensors can monitor various gait parameters, including stride length, stride frequency, stride speed, etc., to truly and objectively monitor and collect data on athletes' gait, which helps to accurately evaluate their gait status and mobility (Bao et al. 2019). Computer vision algorithms analyze the gait of athletes by extracting relevant data, extracting factors such as gait cycle, gait speed, arm swing cycle, and other gait features (Feng et al. 2019). They further analyze the gait of athletes, and extract corresponding feature vectors through algorithm models to achieve automatic recognition and evaluation of movement gait. Although this method has a shorter analysis time,

quantitative analysis techniques can provide more convincing data evidence and provide a more accurate and detailed assessment of athletes' gait status (Kumar et al. 2015).

## 2 Related work

The literature studied human gait on a gait detection system testing platform, selecting 150 sets of gait sets as test samples and using the classic DTW (Dynamic Time Warping) algorithm for recognition (Li et al. 2021). Under the same experimental conditions, by integrating the DTW algorithm with gait parameters, the recognition rate of human gait can be improved to 86.6%. The classic DTW algorithm used in literature for gait recognition has achieved relatively high recognition rates (Yadav and Alam 2018). The DTW algorithm is a very commonly used time series similarity comparison algorithm, which aligns two time series to minimize the distance between them. In gait recognition, the DTW algorithm can effectively compare the similarity between different gaits and achieve gait recognition. The test results show that after extracting human gait features, the recognition rate of human gait using the classic DTW algorithm can reach about 79%. The fusion of DTW algorithm with gait parameters in literature can further improve the accuracy of gait recognition (Wan et al. 2018). By combining the DTW algorithm with gait parameters, the similarity of time series and gait feature parameters can be combined to achieve more accurate recognition of gait. The test results show that under the same experimental conditions, integrating the DTW algorithm with gait parameters can improve the recognition rate of human gait to 86.6%, which is about 7.6 percentage points higher than the classic DTW algorithm.

The literature adopts Kinect devices as visual sensors and designs a human gait testing system (Supuk et al. 2014). The system collects bone data from multiple sets of human motion postures, determines the feature points of the bone data, and combines the clustered data to construct a gait template. Through this step, the system can more accurately recognize human gait and achieve automation of gait recognition. The gait testing system is mainly divided into the following steps. Collect bone data of human motion posture through Kinect devices. Kinect is a device based on a depth camera that can obtain three-dimensional bone information of the human body and achieve real-time tracking, making it very suitable for use in human gait testing systems. The system processes bone data to determine the feature points of the bone data. Generally speaking, key feature points in human gait include joints such as the head, shoulders, buttocks, knees, and ankles, and determining these feature points is crucial for gait recognition. Classify human gait through clustering algorithms and combine data. Clustering algorithms can effectively group data and achieve classification and recognition of gait. Finally, construct a gait template based on the data from each cluster combination. Gait template is a model used to describe human gait features, composed of data from multiple clustering combinations, which can help the system more accurately recognize human gait.

The literature proposes a K-means algorithm based on local spatial information weighting for clustering and segmentation of plantar images (Ahmed et al. 2020). This algorithm divides the foot image into different numbers of foot sub region images, and uses a convolutional neural network (CNN) network to extract the depth features of the sub region images, forming combined features to achieve gait

recognition. Experiments on static datasets have shown that the improved K-means algorithm can effectively segment plantar pressure images, and the segmentation results not only meet the physiological and anatomical structure of the foot, but also fully utilize plantar pressure distribution information. In the gait recognition experiment, the classification accuracy reached 99%, which proves the effectiveness of the improved K-means algorithm in achieving static gait recognition on CNN networks in terms of foot image segmentation compared to traditional methods. The literature produced two gait event flow datasets: DVS128-GAIT and EV-CASIA-B (Filtjens et al. 2020). The DVS128-GAIT dataset was collected in a practical environment, containing gait event flow data from 18 subjects, each of whom underwent multiple walks, totaling approximately 600 sets of data; The EV-CASIA-B dataset was converted from the publicly available gait dataset CASIA-B and contains gait event flow data for 124 individuals, each with 5 walks, totaling approximately 620 sets of data. In the production of the dataset, dynamic visual sensors were used and event based data collection methods were adopted.

### 3 Research on Basic Technology of Fiber Optic Sensors

#### 3.1 Working principle of fiber optic sensors

Based on the characteristics of optical fibers, design reasonable hardware facilities such as optical fibers and receivers, as well as optimized signal processing algorithms to improve the accuracy and reliability of optical signal acquisition. As shown in Fig. 1, a reflective fiber optic displacement sensor is a common photoelectric sensor that utilizes the principle of light reflection between media to measure the displacement of the measured object.

Assuming that the light source fiber and the receiving fiber have the same core diameter  $2r$ , the distance between the receiving fiber and the reflecting surface is  $x$ , and the center distance between the two fibers is  $d$ . According to the geometric relationship, formula (1) can be obtained:

$$\theta = \arcsin \frac{d}{2x}$$

1

The numerical aperture describes the maximum angle range that a fiber can collect and transmit. The larger the numerical aperture, the more light the fiber can collect and have a wider range of receiving angles. In fiber optic transmission, the reflecting cone is cut by the reflecting surface, so the size of the reflecting cone is closely related to the numerical aperture. According to the Pythagorean theorem, it can be concluded that:

$$\tan \theta = \frac{d}{2x}$$

2

Substituting formula (2) into formula (1) yields formula (3):

$$x = \frac{d}{2 \tan(\arcsin NA)}$$

3

## 3.2 Intensity modulation characteristic function

The intensity modulation function is calculated as follows:

$$M = \frac{P_s}{P_0}$$

4

After being reflected by the reflecting surface, the transmitting fiber is ultimately output at a certain light intensity. Due to factors such as attenuation of light intensity in fiber optic transmission, the received light intensity is always lower than the transmitted light intensity. Therefore, in order to evaluate the performance and measurement accuracy of fiber optic sensors, it is necessary to calculate the optical power received by the receiving fiber. The final output light intensity of the sending fiber can be expressed as formula (5):

$$I(r) = \frac{P_0}{\pi \omega^2 (2d)^2} \exp \left[ -\frac{r^2}{\omega^2 (2d)^2} \right]$$

5

When the receiving fiber begins to receive the optical signal emitted by the sensor, the received light intensity can be approximated by the differential method, and the specific expression is as follows:

$$P_s(r, d) = \iint_{S_r} I(r, 2d) dS_r$$

6

By combining formulas (5) and (6), the expression for the optical power received by the receiving fiber can be obtained, as shown in formula (7):

$$P_s = \frac{2(1 - C)P_0}{\pi \omega^2 (2d)^2} \int_{p-r_2}^{\omega(2d)} e^{-\frac{r^2}{\omega^2 (2d)^2}} \arccos \left( \frac{r^2 + p^2 - r_2^2}{2pr} \right) r dr$$

7

The expression for the received optical power of the receiving fiber is formula (8):

$$P_s = \frac{2(1 - C)P_0}{\pi\omega(2d)^2} \int_{\omega(2d)}^{p+r_2} e^{-\frac{r^2}{\omega(2d)^2}} \arccos\left(\frac{r^2 + p^2 - r_2^2}{2pr}\right) r dr$$

8

The intensity modulation characteristic function  $M$  of an optical fiber sensor is related to factors such as the parameters and arrangement structure of the fiber bundle inside the sensor probe, the distance from the probe end face to the measured surface, and so on. In general, the distance between the probe end face and the measured surface is very small, so the intensity modulation characteristic function  $M$  can be expressed in a simple form, i.e. formula (9):

$$M = \frac{P_s}{P_0} = \frac{2(1 - C)}{\pi\omega(2d)^2} \int_{p-r_2}^{p+r_2} e^{-\frac{r^2}{\omega(2d)^2}} \arccos\left(\frac{r^2 + p^2 - r_2^2}{2pr}\right) r dr$$

9

Assuming that the reflecting surface is in an ideal state, that is, the probe end face completely reflects all light, therefore, after a complete transmission cycle, the light intensity value that reaches the probe end face is half of the initial light intensity value. Use formula (10) to represent the light intensity modulation function  $M$ :

$$M = f(r_1, r_2, NA, p, d)$$

10

According to the light intensity modulation characteristic function of a single fiber pair type fiber optic sensor, the intensity modulation function of a reflective intensity modulation type fiber optic sensor is formula (11):

$$M = \frac{M_2}{M_1} = \frac{f_2(r_1, r_3, NA, p_2, d)}{f_1(r_1, r_2, NA, p_1, d)}$$

11

### 3.3 Principle and fabrication of cascaded structure sensors

By calculating the intensity of the interference spectrum using formula (12), information about measuring physical quantities can be obtained.

$$I = I_{co} + I_{cl} + 2\sqrt{I_{co}I_{cl}} \cos(\varphi + \varphi_0)$$

12

In this MZI, the phase difference between the core mode and the cladding mode can be expressed as formula (13).

$$\phi = \frac{2\pi L_{\text{eff}}}{\lambda} \Delta n_{\text{eff}}$$

13

The special feature of this interferometer is that complete interference occurs when the phase difference satisfies the conditions given in formula (14). In this condition,  $m$  represents the order of the interference fringes, and  $\lambda_m$  is the wavelength of the  $M$ -order interference spectrum.

$$\lambda_m = \frac{2L_{\text{eff}}\Delta n_{\text{eff}}}{2m + 1}$$

14

By using formula (15), the free spectral range (FSR) of the interferometer can be calculated, where FSR represents the wavelength difference between the smallest adjacent interference peaks.

$$\text{FSR} = \frac{\lambda_m^2}{L_e \Delta n_{\text{eff}}}$$

15

In sensor structures that utilize hollow silicon tubes to achieve anti resonant reflection effects, as the wavelength gradually deviates, more light is limited to the hollow core of the hollow silicon tube, and its optical loss gradually decreases. When the wavelength is far from the resonant wavelength, light is limited in the guiding core mode and propagates along the single-mode fiber. The  $n$ th resonant wavelength can be represented by formula (16):

$$\lambda_{m'} = \frac{2d}{m'} \sqrt{n_1^2 - n_{\text{air}}^2}$$

16

The intensity of the transmission spectrum can be expressed by formula (17):

$$T_{\text{ARRW}} = \frac{(1 - n_{\text{air}} \cdot n_{\text{HST}})^2 (n_{\text{air}} + n_{\text{HST}})^2}{1 + n_{\text{HST}}^4 - 2n_{\text{HST}}^2} I_{A\eta w'}$$

17

Further derivation of formula (16) leads to the temperature sensitivity formula (18) based on the wavelength shift of the resonant reflection waveguide, in order to calculate the effect of temperature

changes on the wavelength of the resonant reflection waveguide.

$$\frac{\partial \lambda_{m'}}{\partial T} \approx \frac{2n_1 d}{m' \sqrt{n_1^2 - n_{\text{air}}^2}} \cdot \frac{\partial n_1}{\partial T} = \lambda_{\text{mm}} \cdot \frac{n_1}{n_1^2 - n_{\text{air}}^2} \cdot \frac{\partial n_1}{\partial T}$$

18

From Fig. 2, it can be seen that the transmission spectrum of FRSS exhibits a curve similar to a Gaussian distribution, where the trough is located at the center of the wavelength range and does not affect the concave trough of ARRW. Therefore, it is convenient to select the desired trough for fiber optic sensing measurement.

Formula (19) expresses the relationship between wavelength shift and environmental temperature, refractive index.

$$\begin{aligned} \Delta \lambda_B &= k_{T_1} \cdot \Delta T + k_{D_1} \cdot \Delta D \\ \Delta \lambda_A &= k_{T_2} \cdot \Delta T \end{aligned}$$

19

Among them, changes in temperature and refractive index are considered the main interference factors. By experimentally measuring and calculating parameters, and calibrating the measurement results, the accuracy and reliability of the sensor can be improved.

### 3.4 Performance Verification Results of Fiber Optic Sensors

Experimental operations and results conducted to verify the repeatability and stability of the sensor. The experimental group repeated measurements 5 times for each RI, and after each RI was held for 6 minutes, the transmission spectrum was recorded again. Figure 3 shows the position change of the valley wavelength with the variation of RI. As RI changes, the wavelength positions of valleys A and B also change. This indicates that under the changing environment of RI, the measurement results of valleys A and B have a certain sensitivity and stability, which can accurately reflect environmental changes. The results of repeated experiments indicate that the inclination angles of ARRW and FRSS remain basically unchanged in each RI experiment, which means that the proposed sensor has good stability and repeatability, which can meet the needs of practical applications.

Adjust the driving current of the laser to 60mA and heat it for 5 minutes. Read 1000 values collected by the optical power meter and draw the measurement results shown in Fig. 4.

The results in Fig. 4 indicate that the light source output by the semiconductor laser is basically stable, and the selection fully meets the experimental requirements. The experiment used reflective fiber optic sensors and a coordinate measuring instrument to measure the height values of different height steps, and the measurement results are listed in Table 1. By comparing the differences between the three



coordinate measurement data and the reflective fiber optic sensor measurement data, the magnitude of measurement deviation can be obtained.

Table 1

Height values of steps measured by reflective fiber optic sensors and coordinate measuring instruments

Step height (μm)	Coordinate measurement data (μm)	Reflective optical Fiber Sensor Measurement data (μm)	Measurement error (μm)
150	150.568	135.924	14.644
100	99.269	94.884	4.385
90	77.719	62.042	15.677
80	76.254	76.892	-0.638
50	44.940	38.844	6.096

## 4 Gait Analysis Techniques for Athletes Based on Computer Vision Algorithms

### 4.1 Overall structure of gait recognition system

As shown in Fig. 5, this article proposes a gait training system based on human bone information, and designs four modules to implement the system's functions: gait training module, gait recognition module, gait parameter planning module, and gait evaluation module. In this system, human bone information is obtained through sensing devices and real-time data is transmitted to the computer. The computer processes and analyzes bone data to complete the relevant functions of the gait training system.

### 4.2 Model training and noise reduction methods

Model training includes two parts: improved K-means clustering model training and CNN model training. The improvement of K-means clustering model training is mainly aimed at improving the performance of traditional K-means algorithms in high-dimensional data processing. The improved K-means clustering algorithm converts the two-dimensional matrix of plantar pressure images into a sample set, where each sample corresponds to a pixel, and the feature vector is composed of the x and y coordinates of the pixel and the pressure value  $l$  of the pixel. Formula (20) can be used to represent the sample set  $D=\{P_1, P_2, \dots, P_m\}$ , where  $p$  represents the feature vector of each pixel.

$$E = \frac{1}{n} \sum_{i=1}^{k-1} \sum_{p \in C_i} \|p - u_i\|_2^2$$

The objective loss function consists of two terms, the first being the cross entropy loss function. The goal of this section is to minimize the classification error of a given training sample. In the field of deep learning, the cross entropy loss function is usually used in conjunction with the softmax function for multi classification problems. The calculation formula is as follows:

$$J_1(X, W, B) = -\frac{1}{N} \sum_{i=1}^N \langle y^{(i)}, \log \hat{y}^{(i)} \rangle$$

21

In order to reduce the risk of overfitting in the model, weight regularization terms are introduced to limit the size of weights and biases and avoid excessive fluctuations.

$$J_2(W, B) = \sum_{l=1}^L \left( \|w_l\|_F^2 + \|b_l\|_2^2 \right)$$

22

By synthesizing formulas (21) and (22), the full formula of the objective loss function is obtained, as shown in formula (23), where  $w$  and  $b$  are the weights and biases of the neural network, respectively.

$$J = \min (J_1(X, W, B) + \lambda_1 J_2(W, B))$$

23

$$J = \min \left( -\frac{1}{N} \sum_{i=1}^N \langle y^{(i)}, \log \hat{y}^{(i)} \rangle + \lambda_1 \sum_{l=1}^L \left( \|w_l\|_F^2 + \|b_l\|_2^2 \right) \right)$$

24

When calculating the optical flow of an event in the DVS event stream, it is necessary to first remove its polarity and use the information of the plane where the event is located to calculate its motion speed.

$$ax_i + by_i + ct_i + d = 0$$

25

## 4.3 Experimental results of different models and data input forms

The experimental results in Table 2 indicate that using plantar region partitioning can effectively improve the accuracy of gait recognition. The manual region division method and SVM classifier are not as effective as the method proposed in this article, which uses the improved K-means algorithm for clustering segmentation and CNN network for feature extraction. When combining manual region

partitioning with CNN networks, some experimental results even exceeded the results of the proposed method in this study. This indicates that although the manual region division method is difficult to meet the evaluation criteria for foot segmentation, combined with the feature extraction ability of CNN networks, it can also achieve good gait recognition. Therefore, the improved K-means algorithm proposed in this study combines the advantages of CNN network for feature extraction on the basis of foot image segmentation to achieve static gait recognition, enhances the representation ability of foot features, and further improves the accuracy of static gait recognition.

Table 2  
Comparative experimental results of static gait recognition for different regions and models on the test set

classification model	Partition method	Left foot (%)	Right foot (%)	Average value (%)
SVM	No regional division	79.494	74.751	77.123
	Manual 4 zone	83.637	87.098	85.367
	Manual 8 zone	89.381	89.071	89.226
ResNet18	Manual 4 zone	97.303	100.010	98.657
	Manual 8 zone	96.678	98.572	97.625
	(Article) 2 area	90.830	93.283	92.056
	(Article) 3 area	99.508	99.748	99.628
	(Article) 4 area	99.612	99.310	99.461

## 5 Conclusion

This article focuses on the walking movement and gait of humans, analyzing their structure, adjustment mechanism, form, and variation patterns. Fiber optic sensors and computer vision algorithms are used to analyze the gait of athletes, providing scientific reference data and helping them to undergo more scientific training. Walking is the most common form of movement in the human body, and its periodic and regular movements involve the complex coordination of multiple parts of the body. Normal gait requires coordination between the central nervous system and the skeletal muscle system. Once there is damage or disease to the central nervous system or skeletal muscle system, it may lead to abnormal gait. Therefore, scientific analysis and evaluation of gait is very valuable. This article uses fiber optic sensors and computer vision algorithms to analyze the gait of athletes. Fiber optic sensors can monitor the movement of athletes' trunk, pelvis, lower limbs, and upper limb joints and muscle groups in real-time, providing high-precision data. Computer vision algorithms can process and analyze data obtained from sensors, extract gait related features such as gait period, stride length, stride speed, support phase, and swing, and quantitatively evaluate gait.

## Declarations

## Author contributions

Nina Liu has contributed to the paper's analysis, discussion, writing, and revision.

## Fund

The authors have not disclosed any funding.

## Data availability

The data will be available upon request.

## Conflict of interest

The authors declare that they have no competing interests.

## Ethical approval

Not applicable.

## References

1. Silva L M, Stergiou N (2020) The basics of gait analysis. *Biomechanics and gait analysis* 164:231
2. Baker R, Esquenazi A, Benedetti M G, Desloovere K (2016) Gait analysis: clinical facts. *Eur. J. Phys. Rehabil. Med* 52(4):560-574
3. Zeng D, Qu C, Ma T, Qu S, Yin P, Zhao N, Xia Y (2021) Research on a gait detection system and recognition algorithm for lower limb exoskeleton robot. *Journal of the Brazilian Society of Mechanical Sciences and Engineering* 43(6):298
4. Saraji S, Goual L, Piri M, Plancher H (2013) Wettability of supercritical carbon dioxide/water/quartz systems: Simultaneous measurement of contact angle and interfacial tension at reservoir conditions. *Langmuir* 29(23):6856-6866
5. Manssor S A, Sun S, Elhassan M A (2021) Real-time human recognition at night via integrated face and gait recognition technologies. *Sensors* 21(13):4323
6. Verlekar T T, Correia P L, Soares L D (2017) View-invariant gait recognition system using a gait energy image decomposition method. *IET Biometrics* 6(4):299-306
7. Bao Y, Huang Y, Hoehler M S, Chen G (2019) Review of fiber optic sensors for structural fire engineering. *Sensors* 19(4):877
8. Feng X, Jiang Y, Yang X, Du M, Li X (2019) Computer vision algorithms and hardware implementations: A survey. *Integration* 69:309-320
9. Kumar S, Chandra P, Bajpai V, Singh A, Srivastava M, Mishra D K, Kumar B (2015) Rapid qualitative and quantitative analysis of bioactive compounds from *Phyllanthus amarus* using LC/MS/MS techniques. *Industrial Crops and Products* 69:143-152

10. Zeng D, Qu C, Ma T, Qu S, Yin P, Zhao N, Xia Y (2021) Research on a gait detection system and recognition algorithm for lower limb exoskeleton robot. *Journal of the Brazilian Society of Mechanical Sciences and Engineering* 43(6):298
11. Li W, Lu W, Sha X, Xing H, Lou J, Sun H, Zhao Y (2021) Wearable gait recognition systems based on MEMS pressure and inertial sensors: A review. *IEEE Sensors Journal* 22(2):1092-1104
12. Yadav M, Alam M A (2018) Dynamic time warping (dtw) algorithm in speech: a review. *International Journal of Research in Electronics and Computer Engineering* 6(1):524-528
13. Wan C, Wang L, Phoha V V (Eds.) (2018) A survey on gait recognition. *ACM Computing Surveys (CSUR)* 51(5):1-35
14. Supuk T G, Skelin A K, Cic M (2014) Design, development and testing of a low-cost sEMG system and its use in recording muscle activity in human gait. *Sensors* 14(5):8235-8258
15. Prakash C, Kumar R, Mittal N (2018) Recent developments in human gait research: parameters, approaches, applications, machine learning techniques, datasets and challenges. *Artificial Intelligence Review* 49:1-40
16. Subramanian R, Sarkar S (2018) Evaluation of algorithms for orientation invariant inertial gait matching. *IEEE Transactions on Information Forensics and Security* 14(2):304-318
17. Faisal A I, Majumder S, Mondal T, Cowan D, Naseh S, Deen M J (2019) Monitoring methods of human body joints: State-of-the-art and research challenges. *Sensors* 19(11):2629
18. Ahmed M, Seraj R, Islam S M S (2020) The k-means algorithm: A comprehensive survey and performance evaluation. *Electronics* 9(8):1295
19. Filtjens B, Nieuwboer A, D'cruz N, Spildooren J, Slaets P, Vanrumste B (2020) A data-driven approach for detecting gait events during turning in people with Parkinson's disease and freezing of gait. *Gait & Posture* 80:130-136
20. Kececi A, Yildirak A, Ozyazici K, Ayluctarhan G, Agbulut O, Zincir I (2020) Implementation of machine learning algorithms for gait recognition. *Engineering Science and Technology, an International Journal* 23(4):931-937

## Figures

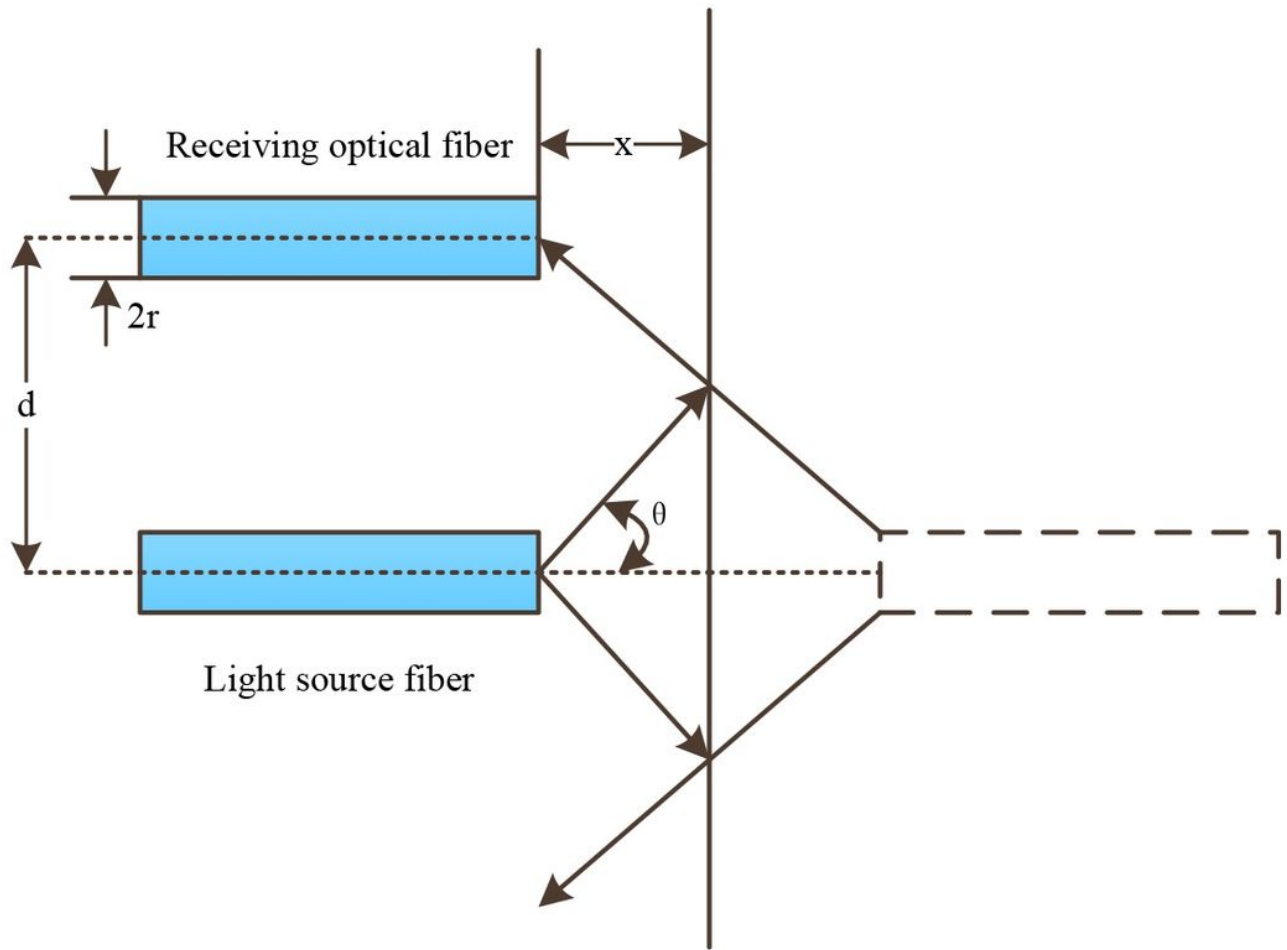


**Figure 1**

Geometric Optical Presentation of Reflective Fiber Optic Displacement Sensor

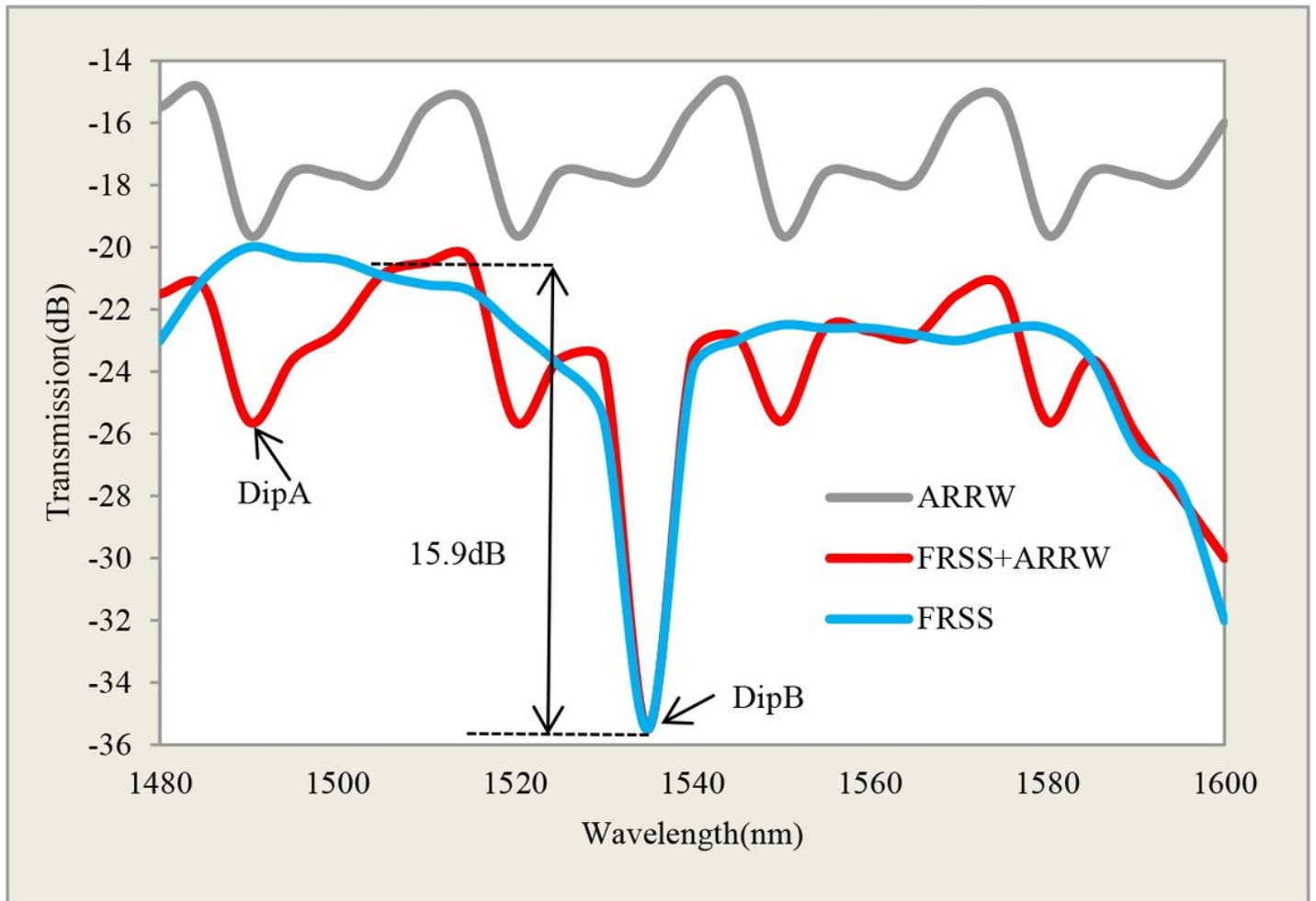


**Figure 2**

Transmission spectra of single FRSS, single ARRW, and cascaded structures

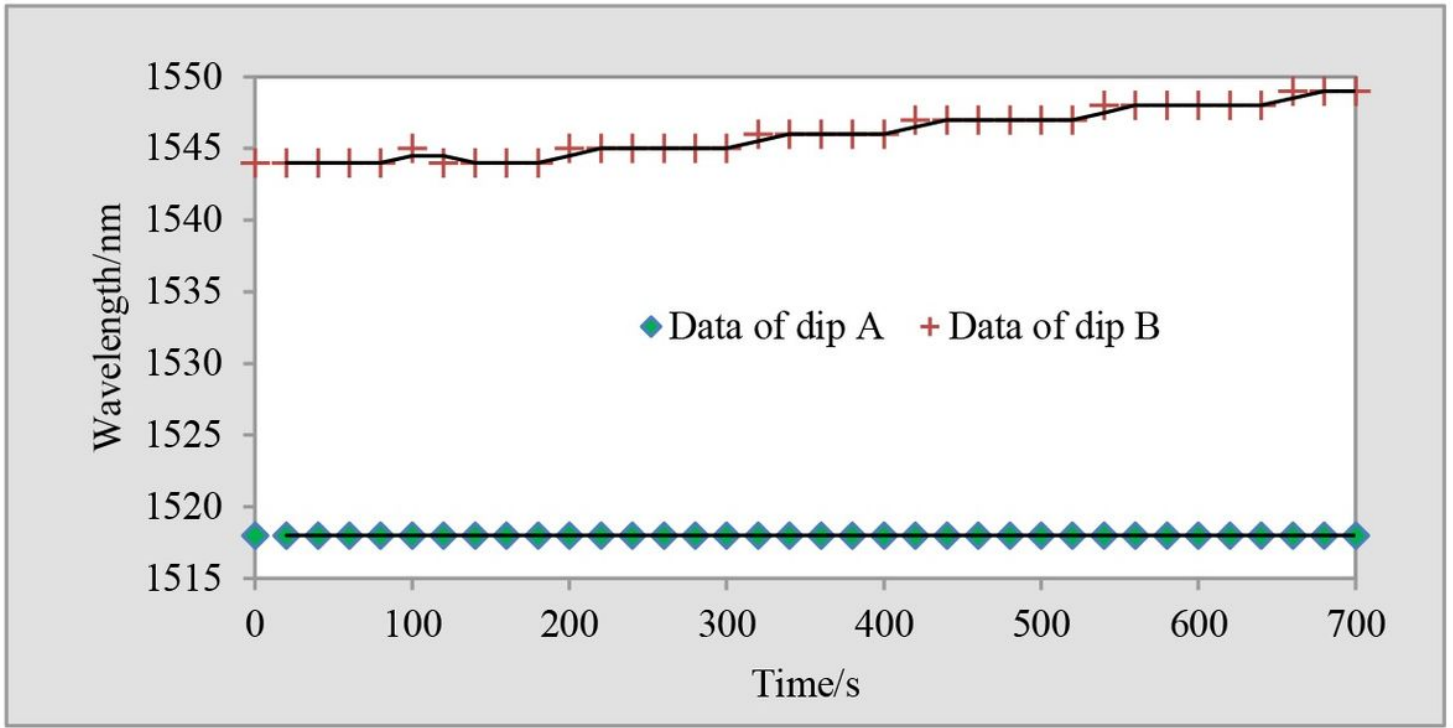


Figure 3

Changes of Valley A and B in Time Domain with Surrounding RI

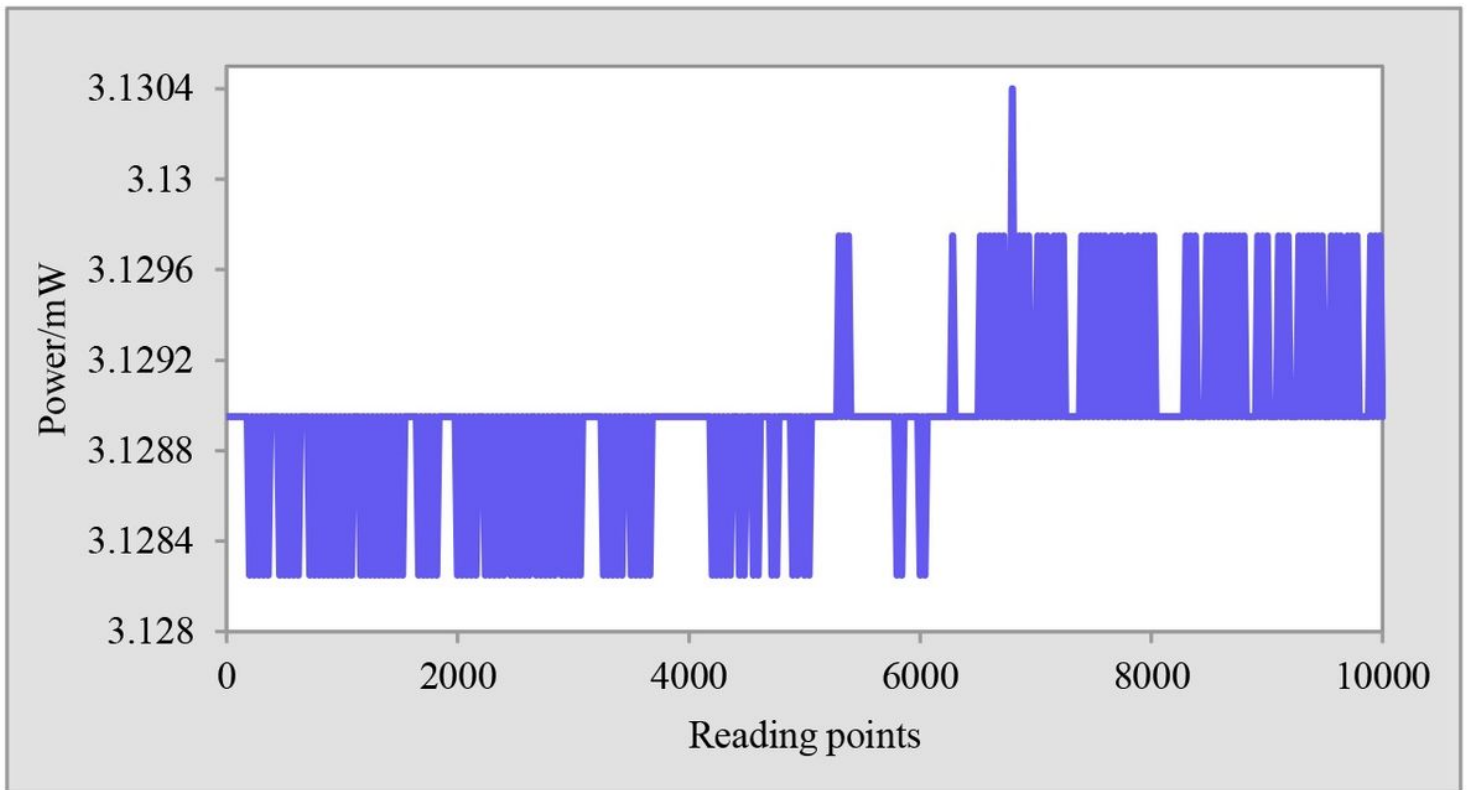


Figure 4



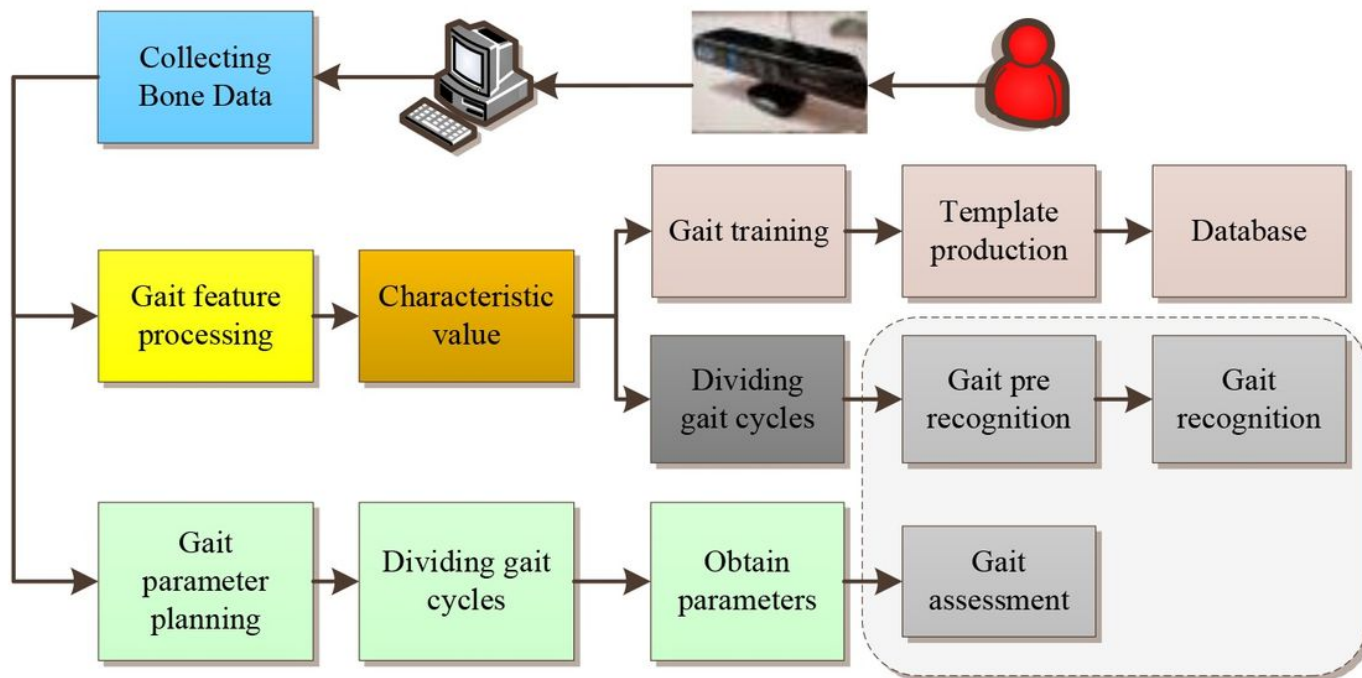


Figure 5

Overall Block Diagram of System Scheme